

Redshift constrain of BL Lac PKS 1424+240

Sarira Sahu^{1*}, D. I. Páez-Sánchez^{2†}, B. Medina-Carrillo^{3‡}, R. de J. Pacheco-Aké^{3§},
G. Sánchez-Colón^{3¶}, Subhash Rajpoot^{4||}

¹*Instituto de Ciencias Nucleares, Universidad Nacional Autónoma de México, Circuito Exterior S/N, C.U., A.P. 70-543, CDMX 04510, México.*

²*Facultad de Ciencias, Universidad Nacional Autónoma de México, Circuito Exterior, C.U., A.P. 70-543, 04510 CDMX, México.*

³*Departamento de Física Aplicada, Centro de Investigación y de Estudios Avanzados del IPN, Unidad Mérida. A.P. 73, Cordemex, Mérida, Yucatán 97310, México.*

⁴*Department of Physics and Astronomy, California State University, 1250 Bellflower Boulevard, Long Beach, CA 90840, USA.*

ABSTRACT

In the period between 2009 and 2015, several very high-energy (VHE > 100 GeV) gamma-ray flaring events from the BL Lac object PKS 1424+240 were observed by the Cerenkov telescopes VERITAS and MAGIC. It had uncertain redshift (z) and using spectroscopical measurement, Paiano et al. (2017) found it to be $z = 0.604$. Using four different extragalactic background light (EBL) models and the photohadronic model, nine independently observed VHE gamma-ray spectra of PKS 1424+240 are analyzed and a global χ^2 fit is performed on all observations to estimate the best-fit value for the redshift for each EBL model. Confidence levels (CL) intervals for the redshift are also estimated using all the EBL models. This method is tested by comparing our analysis with the observed value. It is shown that the photohadronic scenario provides an excellent description of all the observed spectra. It is found that the EBL model of Domínguez et al. (2011) is the one that provides the most restrictive limits on the redshift of PKS 1424+240, but in our analysis, $z = 0.604$ lies within the 3σ CL interval of the EBL model of Saldana-Lopez et al. (2021).

Key words: BL Lacertae objects: general, galaxies: jets, gamma rays: galaxies

1 INTRODUCTION

Blazars are a subclass of active galactic nuclei (AGN), characterized by their non-thermal spectra, originating from a relativistic jet, that is closely aligned with the observer’s line of sight (Urry & Padovani 1995; Acciari et al. 2011). Blazars exhibit rapid variability throughout their entire electromagnetic spectrum. Their spectral energy distributions (SEDs) show a distinctive double-peak structure (Abdo et al. 2010), the first peak arises as synchrotron photons from the propagation of low-energy electrons in the jet magnetic field. However, the second peak can either be from the Compton scattering of high-energy electrons with their self-produced synchrotron photons, a phenomenon known as synchrotron self-Compton (SSC) scattering (Maraschi et al. 1992; Dermer & Schlickeiser 1993; Sikora et al. 1994; Blazejowski et al. 2000; Murase et al. 2012; Gao et al. 2013) or from the external Compton scattering with the photons from the accretion disk, broad-

line regions or the dusty torus (Dermer & Schlickeiser 1993; Sikora et al. 1994; Blazejowski et al. 2000).

PKS 1424+240 was discovered in the 1970s as a radio source (Fanti et al. 1974) and was later identified as a blazar by Impey & Tapia (1988). Later, the source was detected in γ -rays by the *Fermi* Large Area Telescope (LAT; Atwood et al. (2009)). In the spring of 2009, VERITAS reported the observation of VHE gamma-rays from this source (Ong 2009) and, subsequently, it was confirmed by MAGIC (Teshima 2009). Afterwards, several VHE flaring events from PKS 1424+240 were observed between 2009 and 2015. Nonetheless, the frequency of the synchrotron peak ν_{sync}^{peak} for PKS 1424+240 was not directly determined. However, it could be constrained from the optical and the X-ray data and was found to be in the range 10^{15} Hz $\lesssim \nu_{sync}^{peak} \lesssim 10^{17}$ Hz (Acciari et al. 2010). From the classification of the BL Lac objects, we know that this range of ν_{sync}^{peak} classifies the object as high-frequency peaked BL Lac (HBL) (Padovani & Giommi 1996; Abdo et al. 2010; Boettcher et al. 2013).

The non-thermal emission in a BL Lac object dominates over the stellar emission of its host galaxy, making it difficult to correctly estimate the redshift. As a consequence, ambiguities arise in tracing the cosmic evolution, the nature and the understanding of the intrinsic VHE spectrum of the source.

* Contact e-mail: sarira@nucleares.unam.mx

† Contact e-mail: paez@ciencias.unam.mx

‡ Contact e-mail: benjamin.medina@cinvestav.mx

§ Contact e-mail: rodrigo.pacheco@cinvestav.mx

¶ Contact e-mail: gabriel.sanchez@cinvestav.mx

|| Contact e-mail: Subhash.Rajpoot@csulb.edu

Given the fact that VHE photons are dampened by the extragalactic background light (EBL), information of the redshift is essential to investigating the role of the EBL.

EBL models are constructed with the convergence of different approaches as direct measurements, semi analytical models of galaxy formation, analysis of cosmic star formation history, and galaxy luminosity densities with SEDs. The models used in this work belong to the last category and their main difference is the number of galaxy samples employed, which is correlated with the redshift value range of the data output from the model (Saldana-Lopez et al. 2021).

The VHE gamma-ray flux of a blazar observed on Earth is given by (Hauser & Dwek 2001)

$$F_\gamma(E_\gamma) = F_{int}(E_\gamma) e^{-\tau_{\gamma\gamma}(E_\gamma, z)}, \quad (1)$$

where E_γ , F_γ , and F_{int} are the observed VHE photon energy, the observed flux, and the intrinsic flux, respectively. Here, the optical depth $\tau_{\gamma\gamma}$ for the process $\gamma\gamma \rightarrow e^+e^-$ depends on E_γ and the redshift z of the source. The exponential factor in Eq. (1) accounts for the attenuation in the VHE flux due to e^+e^- production (Stecker et al. 1992; Ackermann et al. 2012; Padovani et al. 2017). Thus, knowledge on z is crucial to estimating the intrinsic flux from the observed flux. Well-known and reliable EBL models by Franceschini et al. (2008); Finke et al. (2010); Dominguez et al. (2011); Gilmore et al. (2012); Saldana-Lopez et al. (2021) are employed by Imaging Atmospheric Cerenkov Telescope (IACT) collaborations to analyze the observed VHE γ -ray spectra from objects at different redshifts.

As stated previously, the redshift of HBL PKS 1424+240 is measured spectroscopically with a value $z = 0.604$ (Paiano et al. 2017). However, alternative methods do not provide a definitive result. By making a ‘‘minimum luminosity assumption’’ (host galaxy absolute magnitude to be $M = -21.9$), Scarpa & Falomo (1995) have derived a lower limit of $z > 0.06$, while Sbarufatti et al. (2005) set a limit of $z > 0.67$ by using the average value $M = -22.9$. Acciari et al. (2010) combined the photon index (measured with *Fermi* Large Area Telescope) with EBL models, to estimate the redshift $z = 0.5 \pm 0.1$, with an upper limit of $z < 0.66$ at 95% CL. Comparing the measured and intrinsic VHE spectra due to EBL absorption, an upper limit of 1.19 on the redshift was derived in Yang & Wang (2010). Employing a derived empirical law, describing the relation between the upper limits and the true redshifts, the redshift is estimated to be 0.24 ± 0.05 in Prandini et al. (2010); Prandini et al. (2011). The photometric redshift, obtained through spectral fitting of optical/UV data, has an upper limit of $z < 1.11$ (Rau, A. et al. 2012). Furniss et al. (2013) have given a lower limit, $z \geq 0.6035$, set by the detection of Ly β and Ly γ lines from intervening hydrogen clouds. By multiwavelength spectral characterization and modeling of the blazar, in Ref. Aleksić et al. (2014), a value $z = 0.61 \pm 0.10$ with an upper limit of 0.81 at 2σ is reported. In Ref. Rovero, A. C. et al. (2016), the probability of PKS 1424+240 being a member of a group of galaxies found at $z = 0.6010 \pm 0.003$ was found to be 98%. The observed correlation between the VHE spectral index of blazars and redshift is interpreted as a result of EBL induced absorption effects and the absence of such correlation led to develop a technique to estimate the redshift of distant blazars whose optical spectrum is featureless. For PKS 1424+240,

this technique was employed by Zahoor et al. (2022) and have estimated $z = 0.28 \pm 0.13$ and $z = 0.24 \pm 0.11$.

The multi-zone leptonic models are also used to explain the VHE flaring events. However, one needs to almost double the parameters in these models. Models involving hadrons suffer from low efficiency. For example, in the proton synchrotron scenario, the emission of synchrotron photons by protons in the jet environment is suppressed by a factor of m_p^{-4} , where m_p is the proton mass. Thus, this process requires ultra-high energy proton flux. Also a strong magnetic field is needed, which is unusual in a blazar jet (Mannheim et al. 1991; Mücke & Protheroe 2001; Mücke et al. 2003). There are several other alternative models, such as spine-layer structured jet model and the lepton-hadron hybrid models to explain these spectra (Ghisellini et al. 2005; Tavecchio & Ghisellini 2008; MAGIC Collaboration et al. 2019; Ahnen et al. 2018).

Previously, the photohadronic model (Sahu 2019), has been successfully used to explain the VHE γ -ray spectra of various HBLs and extreme HBLs (EHBLs) (Sahu et al. 2020, 2021, 2022). A new classification scheme was proposed (Sahu et al. 2019) by analyzing the spectral index of several observed VHE γ -ray spectra from HBLs. In the foregoing, the photohadronic model (Sahu 2019) along with four well-known EBL models Saldana-Lopez et al. (2021); Franceschini et al. (2008); Dominguez et al. (2011); Gilmore et al. (2012) are used to analyze nine VHE flaring events of PKS 1424+240 between 2009 and 2015, observed by VERITAS and MAGIC collaborations. By performing a χ^2 global fit to the full set of experimental data points of these VHE spectra, the central values and CL intervals for the redshift of PKS 1424+240 are determined for each EBL model considered.

The plan of this paper is as follows. In Section 2 a brief review of the photohadronic model and its features relevant to the present work is presented. In Section 3 the analysis and results are presented. Finally, Section 4 includes a short summary and discussion.

2 THE PHOTOHADRONIC MODEL

In the photohadronic model, a double jet configuration is assumed during the VHE flaring process (Sahu 2019; Sahu et al. 2019). A double jet configuration has been proposed in earlier works (Ghisellini & Tavecchio 2008; Giannios et al. 2010). In the photohadronic scenario, a compact and constrained narrower jet, with a size R'_f , is formed within the wider jet of size R'_b , $R'_f < R'_b$ (the quantities in the comoving frame are indicated by primes). In the inner region of the jet, the photon density, $n'_{\gamma,f}$, is significantly greater than the photon density in the outer jet region, n'_γ ($n'_{\gamma,f} \gg n'_\gamma$). The photohadronic model is based on the conventional interpretation of the first two peaks in the SED, namely, that the first peak results from the synchrotron radiation emitted by relativistic electrons within the jet environment and the second peak is a consequence of the SSC process. The inner jet moves at a (slightly) higher velocity (with bulk Lorentz factor Γ_{in}) compared to the outer jet (with bulk Lorentz factor Γ_{ext}). For simplicity, it is assumed $\Gamma_{in} \simeq \Gamma_{ext} \equiv \Gamma$ and a common Doppler factor \mathcal{D} (Ghisellini et al. 1998; Krawczynski et al. 2004). For HBLs, we have $\Gamma \simeq \mathcal{D}$.

In the photohadronic scenario, protons are accelerated to very high-energies in the inner jet region, and their dif-

ferential spectrum follows a power-law form, $dN_p/dE_p \propto E_p^{-\alpha}$ (Dermer & Schlickeiser 1993), where E_p is the proton energy and $\alpha \geq 2$ is the proton spectral index. The specific value of α differs, depending on the type of shock encountered. It can be different for non-relativistic shocks, highly relativistic shocks, and oblique relativistic shocks (Keshet & Waxman 2005; Summerlin & Baring 2012). The interaction of these high-energy protons with the SSC background seed photons in the inner jet region results in the production of the Δ -resonance through the process $p + \gamma \rightarrow \Delta^+$. The Δ -resonance decays to π^0 and π^+ with different probabilities. Although the direct single pion production and the multi-pion production processes contribute, they are less efficient in the energy range under consideration (Mücke et al. 1999; Owen et al. 2018). Such contributions are neglected in the present work. Finally, the neutral pion decays to γ -rays and the π^+ to neutrinos (Sahu et al. 2012). In the photohadronic scenario, the γ -rays generated from π^0 decay are blue-shifted to VHE γ -rays and are detected on Earth. The positrons produced from π^+ decay will emit synchrotron photons.

The observed VHE γ -ray energy E_γ and the seed photon energy ϵ_γ satisfy the condition (Sahu 2019; Sahu et al. 2019)

$$E_\gamma \epsilon_\gamma \simeq 0.032 \frac{\mathcal{D}^2}{(1+z)^2} \text{ GeV}^2. \quad (2)$$

In the above process, the VHE photon carries approximately 10% of the proton energy, $E_p = 10E_\gamma$. Given the inaccessible nature of the inner jet region and the lack of direct means to estimate the photon density within it, a scaling relationship between the inner and the outer jet regions is assumed, which can be expressed as (Sahu et al. 2016)

$$\frac{n'_{\gamma,f}(\epsilon_{\gamma,1})}{n'_{\gamma,f}(\epsilon_{\gamma,2})} \simeq \frac{n'_\gamma(\epsilon_{\gamma,1})}{n'_\gamma(\epsilon_{\gamma,2})}. \quad (3)$$

In the above equation, the left-hand side represents the unknown, while the right-hand side is known. This equation is employed to express the unknown photon density in the inner region in terms of the known photon density in the outer region.

The intrinsic γ -ray flux from the π^0 decay is deduced to be

$$F_\gamma(E_\gamma) \equiv E_\gamma^2 \frac{dN(E_\gamma)}{dE_\gamma} \propto E_p^2 \frac{dN(E_p)}{dE_p} n'_{\gamma,f}. \quad (4)$$

By taking into account the seed photon density and the proton flux, the intrinsic flux can be expressed as

$$F_{int}(E_\gamma) = F_0 \left(\frac{E_\gamma}{\text{TeV}} \right)^{-\delta+3}. \quad (5)$$

By putting this in Eq. (1), the observed flux is determined to be

$$F_\gamma(E_\gamma) = F_0 \left(\frac{E_\gamma}{\text{TeV}} \right)^{-\delta+3} e^{-\tau_{\gamma\gamma}(E_\gamma, z)}, \quad (6)$$

where the spectral index $\delta = \alpha + \beta$. The component β represents the power spectrum of the seed photons in the low energy tail region of the SSC spectrum. The normalization factor F_0 can be determined from the observed data. The value of δ is considered as the only free parameter in the photohadronic model (Sahu et al. 2019). As can be seen from

Eq.(6), in the photohadronic model the curvature in the spectrum, if any, can be taken care of by the exponential term (Acciari et al. 2019).

It is important to note that the photohadronic process works well for $E_\gamma \gtrsim 100$ GeV. Below this energy, the leptonic processes such as the electron synchrotron mechanism and the SSC process have the dominant contribution to the multiwavelength SED.

3 ANALYSIS AND RESULTS

In the analysis of the VHE gamma-ray spectra of PKS 1424+240, the EBL corrections are taken care of by the use of four well-known EBL models. For convenience, the EBL models are referred to as Saldana (Saldana-Lopez et al. 2021), Franceschini (Franceschini et al. 2008), Domínguez (Domínguez et al. 2011), and Gilmore (Gilmore et al. 2012). Also for convenience, each observation is named according to the telescope and the year of observation. The observations by VERITAS in 2009 (from MJD 54881 to MJD 55003) are named as VO09-I for the time averaged spectrum analysis and as VO09-II for the analysis of the VHE γ -ray spectrum. In Table 1 we have listed details about all the observations.

In accordance with the classification scheme given by Sahu et al. (2019), the VHE emission states of a HBL are defined according to the δ value. The emission state is considered very high when $2.5 \leq \delta \leq 2.6$. The high emission state corresponds to $2.6 < \delta < 3.0$ and $\delta = 3.0$ implies the low emission state. Since PKS 1424+240 is a HBL, δ must be constrained to lie in the range $2.5 \leq \delta \leq 3.0$.

The duration of time observed during each observation period by VERITAS and MAGIC are between two to five months. Thus, the observed spectra are the average spectra. It is very important to note that these observation periods are too long for a spectrum to be in a very high emission state or high emission state. Also, the average spectrum of a long observation is always in a low emission state which corresponds to $\delta = 3.0$. Thus, for further analysis to all the nine spectra, we fixed the spectral index to $\delta = 3.0$.

For our analysis and to find the best fits to the observed VHE-spectra for a given EBL model, the EBL model is implemented in the photohadronic model and a global χ^2 fit is performed on all the data points by simultaneously varying the redshift z (common to all observations) and the corresponding normalization constants F_0 of each of the nine independent observations. The global fitting procedure is repeated for the other three EBL models too to find the best-fit value of the redshift z of the HBL PKS 1424+240 and the normalization F_0 of the photohadronic model. The redshift CL intervals at 1σ , 2σ , and 3σ , are then calculated for each of the four EBL models considered.

The best fit values for the normalization constants F_0 , corresponding to each observation and for the four EBL models, are given in Table 2. One can observe that for a given observation, the F_0 value is very similar in all the EBL models. This clearly shows that all the EBL models are also similar to each other. Analogously, the best-fit values for the redshift z and their CL intervals at 1σ , 2σ , and 3σ , are calculated which are shown in Table 3. With 42 degrees of freedom (52 experimental data points considered and 10 free param-

eters), values of minimum χ^2 obtained for the global fit are 61.8, 64.74, 66.47, and 63.51 for the EBL models of Saldana, Franceschini, Domínguez, and Gilmore, respectively. The use of a different EBL model predicts different CL intervals of z for each observed VHE spectrum. The photohadronic model with the EBL model of Domínguez provides the most restrictive intervals on the redshift, $z = 0.689$ the central value with $0.650 \leq z \leq 0.724$ at 1σ , $0.622 \leq z \leq 0.748$ at 2σ , and $0.610 \leq z \leq 0.758$, at 3σ . Although, the least restrictive intervals on z are obtained with the EBL model of Saldana, the measured value of $z = 0.604$ lies within the 3σ CL interval of this model.

Fits to the nine observed VHE spectra of PKS 1424+240 are displayed in Fig. 1, where, the best-fit parameters for the EBL model of Saldana (given in Tables 2 and 3) are used. The fits to the VHE spectra using the Domínguez, Franceschini, and Gilmore EBL models are omitted because, visually, there is no discernible difference from one EBL model to another. For comparison, all the four EBL models are used to best fit the spectrum of VO13 which is shown in Fig. 2. All the four EBL models fit very well to the data. However, for $E_\gamma \gtrsim 0.3$ TeV we observe a small discrepancy. The Saldana EBL model is implemented in the photohadronic model to determine the butterfly 3σ -CL regions for the nine observed spectra, which are also shown in Fig. 1. Plots of CL regions with the other three EBL models considered are omitted. For comparison, the redshift of PKS 1424+240 estimated by different authors and the spectroscopic measurement are summarized in Table 4.

4 SUMMARY AND DISCUSSION

In this work, the photohadronic model is used in conjunction with the EBL models of Saldana, Franceschini, Domínguez, and Gilmore, to impose stringent constraints on the redshift of PKS 1424+240. This is done by analyzing nine different VHE spectra, independently observed by VERITAS and MAGIC telescopes in the period between 2009 and 2015. Since the photohadronic model (Sahu 2019; Sahu et al. 2019) has demonstrated its effectiveness in constraining the redshift of various HBLs with unknown z values (Sahu et al. 2023), it is employed again to analyze the nine VHE spectra of PKS 1424+240 to constrain its redshift.

The observation period for each spectrum varies between two to five months, too long for a spectrum to be in a very high emission state or in a high emission state. It is observed that all the nine VHE emissions of the HBL PKS 1424+240 were in low emission states ($\delta = 3.0$). With this information, for the analysis, a global χ^2 fit is performed by simultaneously varying the redshift z of the object and the normalization constants F_0 of each one of the nine independent observations, to find the best fit to the observed VHE spectra for a given EBL model. This procedure is repeated for all the other three EBL models to find the corresponding best fit values of z and the parameters F_0 . Using the best fit values of the redshift z and the F_0 's, the redshift CL intervals at 1σ , 2σ , and 3σ , for each one of the four EBL models considered are calculated.

Our analysis shows that the EBL model of Dominguez et al. (2011) provides the most restrictive limits on the redshift and the least restrictive intervals on z are obtained with the EBL model of Saldana-Lopez et al. (2021). However, the

measured value of $z = 0.604$ (Paiano et al. 2017) lies within the 3σ CL interval of the EBL model of Saldana-Lopez et al. (2021) only.

ACKNOWLEDGEMENTS

We thank the reviewer for her/his constructive remarks which helped us to improved the manuscript substantially. The work of S.S. is partially supported by DGAPA-UNAM (México) Project No. IN103522. B. M-C, R. de J. P-A, and G. S-C, would like to thank CONAHCYT (México) for partial support. Partial support from CSU-Long Beach is gratefully acknowledged.

DATA AVAILABILITY

No new data were generated or analysed in support of this research.

REFERENCES

- Abdo A. A., et al., 2010, *ApJ*, 716, 30
 Acciari V. A., et al., 2010, *ApJL*, 708, L100
 Acciari V. A., et al., 2011, *ApJ*, 729, 2
 Acciari V. A., et al., 2019, *MNRAS*, 486, 4233
 Ackermann M., et al., 2012, *Science*, 338, 1190
 Ahnen M. L., et al., 2018, *A&A*, 620, A181
 Aleksić J., et al., 2014, *A&A*, 567, A135
 Archambault S., et al., 2014, *ApJ*, 785, L16
 Atwood W. B., et al., 2009, *ApJ*, 697, 1071
 Blazejowski M., Sikora M., Moderski R., Madejski G., 2000, *ApJ*, 545, 107
 Boettcher M., Reimer A., Sweeney K., Prakash A., 2013, *ApJ*, 768, 54
 Dermer C. D., Schlickeiser R., 1993, *ApJ*, 416, 458
 Dominguez A., et al., 2011, *MNRAS*, 410, 2556
 Fanti C., Fanti R., Ficarra A., Padrielli L., 1974, *A&AS*, 18, 147
 Finke J. D., Razzaque S., Dermer C. D., 2010, *ApJ*, 712, 238
 Franceschini A., Rodighiero G., Vaccari M., 2008, *A&A*, 487, 837
 Furniss A., et al., 2013, *ApJL*, 768, L31
 Gao H., Lei W.-H., Zhang B., 2013, *MNRAS*, 435, 2520
 Ghisellini G., Tavecchio F., 2008, *MNRAS*, 387, 1669
 Ghisellini G., Celotti A., Fossati G., Maraschi L., Comastri A., 1998, *MNRAS*, 301, 451
 Ghisellini G., Tavecchio F., Chiaberge M., 2005, *A&A*, 432, 401
 Giannios D., Uzdensky D. A., Begelman M. C., 2010, *MNRAS*, 402, 1649
 Gilmore R. C., Somerville R. S., Primack J. R., Domínguez A., 2012, *MNRAS*, 422, 3189
 Hauser M. G., Dwek E., 2001, *ARA&A*, 39, 249
 Impey C. D., Tapia S., 1988, *ApJ*, 333, 666
 Keshet U., Waxman E., 2005, *PRL*, 94, 111102
 Krawczynski H., et al., 2004, *ApJ*, 601, 151
 MAGIC Collaboration et al., 2019, *MNRAS*, 490, 2284
 Mannheim K., Biermann P. L., Kruells W. M., 1991, *A&A*, 251, 723

Table 1. Information of the PKS 1424+240 observations employed in this work. Name and instrument of the observation is presented in the first and second column, respectively. Start date, end date, period span (in MJD), and duration of the observation are found in the third, fourth, fifth, and sixth columns, respectively. The work in which each observation period data is featured is presented in the seventh column.

Observation	Instrument	Start date	End date	Period (MJD)	Duration (h)	Reference
VO09-I	VERITAS	19/02/2009	21/06/2009	54881 - 55003	37.3	Acciari et al. (2010)
VO09-II						
MO09	MAGIC	17/04/2009	23/06/2009	54938 - 55005	12.5	Aleksić et al. (2014)
MO10	MAGIC	14/03/2010	19/04/2009	55269 - 55305	11.6	Aleksić et al. (2014)
VO11	VERITAS	06/02/2011	30/05/2011	55598 - 55711	14	Archambault et al. (2014)
MO11	MAGIC	24/04/2011	08/05/2011	55675 - 55689	9.5	Aleksić et al. (2014)
VO13	VERITAS	11/02/2013	04/05/2013	56334 - 56447	67	Archambault et al. (2014)
MO14	MAGIC	23/03/2014	18/06/2014	56739 - 56826	28.19	Acciari et al. (2019)
MO15	MAGIC	22/01/2015	13/06/2015	57044 - 57186	20.9	Acciari et al. (2019)

Table 2. Estimated values for the normalization constant F_0 (in units of 10^{-11} erg cm $^{-2}$ s $^{-1}$) of the photohadronic model obtained from the best fits to the VHE spectra of PKS 14+240 for four EBL models are presented in the third column. Refer to the main text for the different observations given in the first column and for the different EBL models mentioned in the second column. The spectral index $\delta = 3.0$ (low emission state) is used.

Observation	EBL Model	F_0
VO09-I	Saldana	1.420
	Franceschini	1.271
	Domínguez	1.337
	Gilmore	1.421
VO09-II	Saldana	1.767
	Franceschini	1.593
	Domínguez	1.683
	Gilmore	1.776
MO09	Saldana	3.590
	Franceschini	3.257
	Domínguez	3.426
MO10	Gilmore	3.624
	Saldana	1.191
	Franceschini	1.074
VO11	Domínguez	1.126
	Gilmore	1.194
	Saldana	1.840
MO11	Franceschini	1.649
	Domínguez	1.736
	Gilmore	1.840
VO13	Saldana	3.162
	Franceschini	2.855
	Domínguez	2.996
MO14	Gilmore	3.175
	Saldana	1.034
	Franceschini	0.931
MO15	Domínguez	0.981
	Gilmore	1.037
	Saldana	1.907
MO15	Franceschini	1.709
	Domínguez	1.797
	Gilmore	1.913
MO15	Saldana	1.462
	Franceschini	1.312
	Domínguez	1.381
	Gilmore	1.460

Table 3. Estimated values for the redshift in the photohadronic model obtained from the global χ^2 fit to the VHE spectra of the HBL PKS 1424+240. Refer to the main text for the different EBL models mentioned in the first column. The redshift z is given in the second column. The redshift CL intervals at 1σ , 2σ , and 3σ are shown in the third, the fourth, and the fifth columns for each EBL model employed, respectively.

EBL Model	Redshift	Redshift CL intervals		
	z	1σ	2σ	3σ
Saldana	0.660	(0.626, 0.724)	(0.607, 0.756)	(0.597, 0.770)
Franceschini	0.679	(0.639, 0.722)	(0.616, 0.749)	(0.605, 0.762)
Domínguez	0.689	(0.650, 0.724)	(0.622, 0.748)	(0.610, 0.758)
Gilmore	0.727	(0.685, 0.770)	(0.661, 0.798)	(0.650, 0.812)

Table 4. Summary of the spectroscopic measurement and estimations by different authors for the redshift value z of PKS 1424+240. The redshift measurement and estimated interval limits, or central values with uncertainties, are given in the second column, the third column indicates the method used to determine the redshift. Corresponding references are given in the fourth column.

n	Redshift	Method	Reference
1	$z = 0.604$	Spectroscopic measurement	Paiano et al. (2017)
2	$0.06 < z$	Minimum luminosity assumption	Scarpa & Falomo (1995)
3	$0.67 < z$	Average luminosity value	Sbarufatti et al. (2005)
4	$z = 0.5 \pm 0.1$	Photon index – EBL models combination	Acciari et al. (2010)
5	$z < 0.66$ at 95% CL	Photon index – EBL models combination	Acciari et al. (2010)
6	$z < 1.19$	Measured – intrinsic VHE spectra comparison	Yang & Wang (2010)
7	$z = 0.24 \pm 0.05$	Upper limits – true redshifts relationship	Prandini et al. (2010); Prandini et al. (2011)
8	$z < 1.11$	Spectral fitting of optical/UV data	Rau, A. et al. (2012)
9	$0.6035 < z$	Ly β and Ly γ lines detection	Furniss et al. (2013)
10	$z = 0.61 \pm 0.10$	Multiwavelength spectral characterization	Aleksić et al. (2014)
11	$z < 0.81$ at 2σ	Multiwavelength spectral characterization	Aleksić et al. (2014)
12	$z = 0.6010 \pm 0.003$	Member of a group of galaxies probability	Rovero, A. C. et al. (2016)
13	$z = 0.28 \pm 0.13$	VHE spectral index – redshift correlation	Zahoor et al. (2022)
14	$z = 0.24 \pm 0.11$	VHE spectral index – redshift correlation	Zahoor et al. (2022)
15	$0.597 < z < 0.770$ at 95% CL	Global fit to independent observations	Present work (EBL Saldana)

- Maraschi L., Ghisellini G., Celotti A., 1992, *ApJL*, **397**, L5
- Mücke A., Rachen J. P., Engel R., Protheroe R. J., Stanev T., 1999, *PASA*, **16**, 160
- Mücke A., Protheroe R. J., Engel R., Rachen J. P., Stanev T., 2003, *Astroparticle Physics*, **18**, 593
- Murase K., Dermer C. D., Takami H., Migliori G., 2012, *ApJ*, **749**, 63
- Mücke A., Protheroe R., 2001, *Astroparticle Physics*, **15**, 121
- Ong R. A., 2009, *ATel*, **2084**, 1
- Owen E. R., Jacobsen I. B., Wu K., Surajbali P., 2018, *MNRAS*, **481**, 666
- Padovani P., Giommi P., 1996, *MNRAS*, **279**, 526
- Padovani P., et al., 2017, *A&AR*, **25**, 2
- Paiano S., Landoni M., Falomo R., Treves A., Scarpa R., Righi C., 2017, *The Astrophysical Journal*, **837**, 144
- Prandini E., Bonoli G., Maraschi L., Mariotti M., Tavecchio F., 2010, *MNRAS Letters*, **405**, L76
- Prandini E., Bonoli G., Maraschi L., Mariotti M., Tavecchio F., 2011, *Nuovo Cimento C Geophysics Space Physics C*, **34**, 241
- Rau, A. et al., 2012, *A&A*, **538**, A26
- Rovero, A. C. Muriel, H. Donzelli, C. Pichel, A. 2016, *A&A*, **589**, A92
- Sahu S., 2019, *Rev. Mex. Fis.*, **65**, 307
- Sahu S., Zhang B., Fraija N., 2012, *Phys. Rev. D*, **85**, 043012
- Sahu S., Miranda L. S., Rajpoot S., 2016, *EPJ. C*, **76**, 127
- Sahu S., Fortín C. E. L., Nagataki S., 2019, *ApJ*, **884**, L17
- Sahu S., López Fortín C. E., Castañeda Hernández L. H., Nagataki S., Rajpoot S., 2020, *ApJ*, **901**, 132
- Sahu S., López Fortín C. E., Valadez Polanco I. A., Rajpoot S., 2021, *ApJ*, **914**, 120
- Sahu S., Valadez Polanco I. A., Rajpoot S., 2022, *MNRAS*, **515**, 5235
- Sahu S., Medina-Carrillo B., Sánchez-Colón G., Rajpoot S., 2023, *MNRAS*, **522**, 5840
- Saldana-Lopez A., et al., 2021, *MNRAS*, **507**, 5144
- Sbarufatti B., Treves A., Falomo R., 2005, *ApJ*, **635**, 173
- Scarpa R., Falomo R., 1995, *A&A*, **303**, 656
- Sikora M., Begelman M. C., Rees M. J., 1994, *ApJ*, **421**, 153
- Stecker F. W., de Jager O. C., Salamon M. H., 1992, *ApJ*, **390**, L49
- Summerlin E. J., Baring M. G., 2012, *ApJ*, **745**, 63
- Tavecchio F., Ghisellini G., 2008, *MNRAS*, **385**, L98
- Teshima M., 2009, *ATel*, **2098**, 1
- Urry C. M., Padovani P., 1995, *PASP*, **107**, 803
- Yang J., Wang J., 2010, *PASJ*, **62**, L23
- Zahoor M., Sahayanathan S., Zahir S., Iqbal N., Manzoor A., Bhatt N., 2022, *MNRAS*, **511**, 994

This paper has been typeset from a $\text{\TeX}/\text{\LaTeX}$ file prepared by the author.

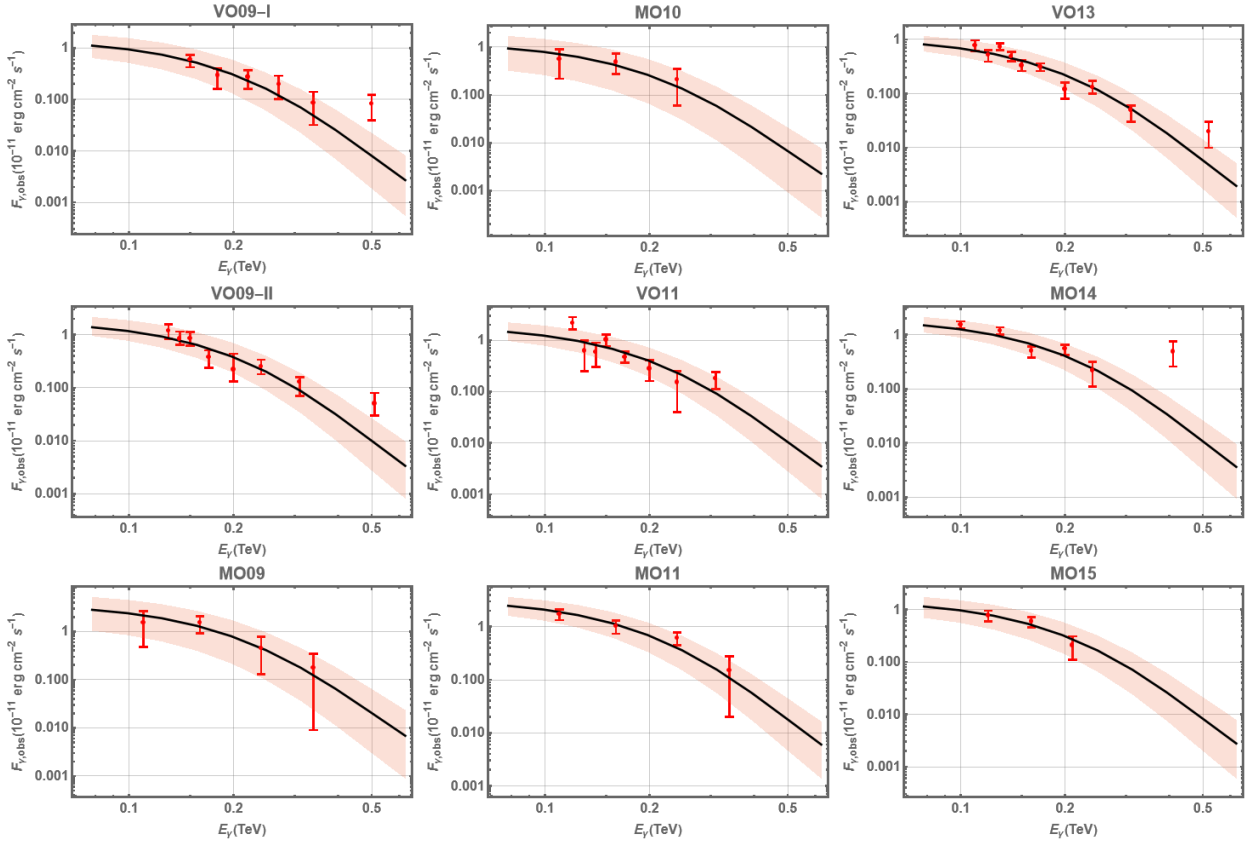


Figure 1. Fits to the nine observed VHE γ -ray spectra of PKS 1424+240 using the photohadronic model with the EBL model of Saldana (solid black curves). All these flaring events are in low emission state corresponding to $\delta = 3.0$. Here, $z = 0.660$, and the corresponding F_0 's are given in Table 2. Plots of the 3σ -CL regions to all the nine observed VHE spectra are also shown.

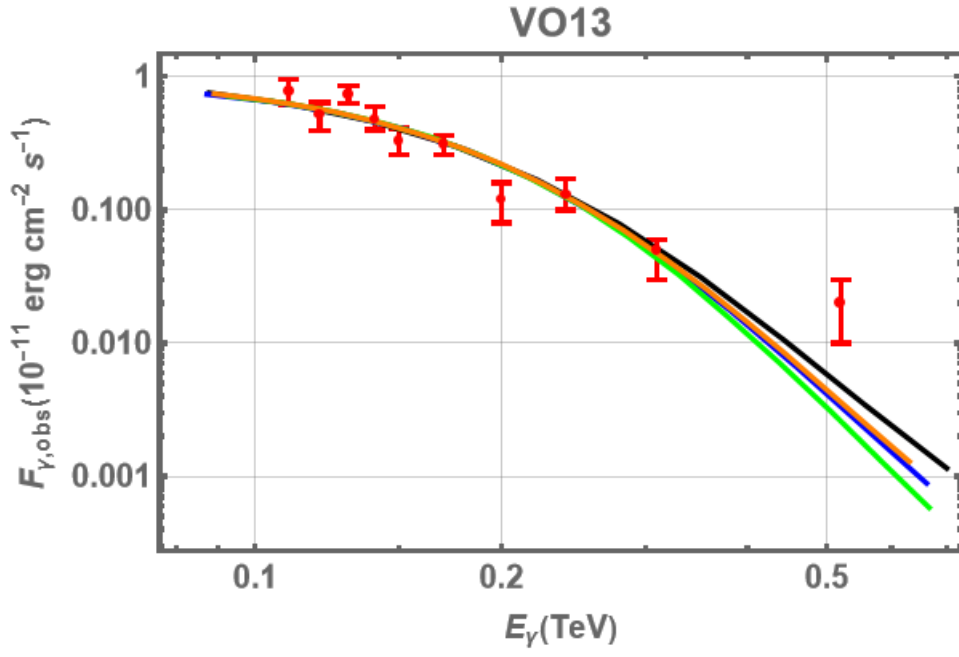


Figure 2. Photohadronic model fits to the observed VHE spectrum VO13 of PKS 1424+240 to illustrate the comparison of different EBL models: Saldana (black), Franceschini (blue), Domínguez (green), and Gilmore (orange). Corresponding values of the normalization constants F_0 and the redshift z are provided in Tables 1 and 2, respectively. As mentioned, for VO13, the VHE flaring is in low emission state, $\delta = 3.0$.